

# UCLA

## UCLA Previously Published Works

### Title

A Cross-Species Neuroimaging Study of Sex Chromosome Dosage Effects on Human and Mouse Brain Anatomy.

### Permalink

<https://escholarship.org/uc/item/4mj26951>

### Journal

The Journal of Neuroscience, 43(8)

### Authors

Guma, Elisa  
Beauchamp, Antoine  
Liu, Siyuan  
et al.

### Publication Date

2023-02-22

### DOI

10.1523/JNEUROSCI.1761-22.2022

Peer reviewed

# A Cross-Species Neuroimaging Study of Sex Chromosome Dosage Effects on Human and Mouse Brain Anatomy

Elisa Guma,<sup>1</sup> Antoine Beauchamp,<sup>2,3,4</sup> Siyuan Liu,<sup>1</sup> Elizabeth Levitis,<sup>1</sup> Liv S. Clasen,<sup>1</sup> Erin Torres,<sup>1</sup> Jonathan Blumenthal,<sup>1</sup> Francois Lalonde,<sup>1</sup> Lily R. Qiu,<sup>2,3</sup> Haley Hrcncir,<sup>6</sup> Allan MacKenzie-Graham,<sup>5</sup> Xia Yang,<sup>6</sup> Arthur P. Arnold,<sup>6</sup> Jason P. Lerch,<sup>2,3,4,7\*</sup> and Armin Raznahan<sup>1\*</sup>

<sup>1</sup>Section on Developmental Neurogenomics, Human Genetics Branch, National Institute of Mental Health, Bethesda, 20892, Maryland, <sup>2</sup>Mouse Imaging Centre, Toronto, Ontario M5T 3H7, Canada, <sup>3</sup>The Hospital for Sick Children, Toronto, Ontario M5G 1X8, Canada, <sup>4</sup>Department of Medical Biophysics, University of Toronto, Toronto, Ontario M5G 1L7, Canada, <sup>5</sup>Department of Neurology, David Geffen School of Medicine, University of California, Los Angeles, Los Angeles, California 90095, <sup>6</sup>Department of Integrative Biology and Physiology, University of California, Los Angeles, Los Angeles, California 90095, and <sup>7</sup>Wellcome Centre for Integrative Neuroimaging, University of Oxford, Oxford, OX3 9DU, United Kingdom

All eutherian mammals show chromosomal sex determination with contrasting sex chromosome dosages (SCDs) between males (XY) and females (XX). Studies in transgenic mice and humans with sex chromosome trisomy (SCT) have revealed direct SCD effects on regional mammalian brain anatomy, but we lack a formal test for cross-species conservation of these effects. Here, we develop a harmonized framework for comparative structural neuroimaging and apply this to systematically profile SCD effects on regional brain anatomy in both humans and mice by contrasting groups with SCT (XXY and XYY) versus XY controls. Total brain size was substantially altered by SCT in humans (significantly decreased by XXY and increased by XYY), but not in mice. Robust and spatially convergent effects of XXY and XYY on regional brain volume were observed in humans, but not mice, when controlling for global volume differences. However, mice do show subtle effects of XXY and XYY on regional volume, although there is not a general spatial convergence in these effects within mice or between species. Notwithstanding this general lack of conservation in SCT effects, we detect several brain regions that show overlapping effects of XXY and XYY both within and between species (cerebellar, parietal, and orbitofrontal cortex), thereby nominating high priority targets for future translational dissection of SCD effects on the mammalian brain. Our study introduces a generalizable framework for comparative neuroimaging in humans and mice and applies this to achieve a cross-species comparison of SCD effects on the mammalian brain through the lens of SCT.

**Key words:** comparative neuroimaging; cross-species homology; magnetic resonance imaging; neuroanatomy; sex chromosome aneuploidy; sex chromosome trisomy

## Significance Statement

Sex chromosome dosage (SCD) affects neuroanatomy and risk for psychopathology in humans. Performing mechanistic studies in the human brain is challenging but possible in mouse models. Here, we develop a framework for cross-species neuroimaging analysis and use this to show that an added X- or Y-chromosome significantly alters human brain anatomy but has muted effects in the mouse brain. However, we do find evidence for conserved cross-species impact of an added chromosome in the fronto-parietal cortices and cerebellum, which point to regions for future mechanistic dissection of sex chromosome dosage effects on brain development.

Received Sep. 12, 2022; revised Dec. 12, 2022; accepted Dec. 22, 2022.

Author contributions: E.G., A.M.-G., X.Y., A.P.A., J.P.L., and A.R. designed research; E.G., S.L., E.L., L.S.C., E.T., J.B., F.L., L.R.Q., H.H., and A.R. performed research; A.P.A. and J.P.L. contributed unpublished reagents/analytic tools; E.G., A.B., S.L., E.L., and J.P.L. analyzed data; E.G. wrote the first draft of the paper; E.G., A.B., S.L., E.L., X.Y., A.P.A., J.P.L., and A.R. edited the paper; E.G. wrote the paper.

This study was supported by the National Institute of Mental Health Intramural Research Program Project Funding Grant 1ZIAMH002949-03 (clinical trials identifier: NCT00001246; clinicaltrials.gov; protocol: 89-M-0006) and the National Institute of Child Health and Disease Grant R01HD100298. E.G. also received salary support from the Fonds de Recherche du Québec en Santé.

We thank Allysa Warling and Ethan Whitman for their contributions to the collection of the human XXY and XYY data.

\*J.P.L. and A.R. contributed equally to this work.

The authors declare no competing financial interests.

Correspondence should be addressed to Elisa Guma at [elisa.guma@nih.gov](mailto:elisa.guma@nih.gov) or Armin Raznahan at [raznahan@mail.nih.gov](mailto:raznahan@mail.nih.gov) or Jason P. Lerch at [jason.lerch@ndcn.ox.ac.uk](mailto:jason.lerch@ndcn.ox.ac.uk).

<https://doi.org/10.1523/JNEUROSCI.1761-22.2022>

Copyright © 2023 the authors

## Introduction

Several independent lines of research provide evidence for sex chromosome dosage (SCD) effects on mammalian brain anatomy. In humans, sex chromosome aneuploidies (SCA), a group of neurogenetic disorders characterized by carriage of an abnormal number of X- and/or Y-chromosomes, are associated with significant neuroanatomical alterations. More specifically, abnormal SCD influences both total and regional volume of the human brain. Furthermore, neuroimaging studies of “four core genotype” mice, a model that allows for chromosome dosage and gonadal background to be uncoupled, have identified SCD effects wherein XX and XY groups differ in regional brain anatomy independent of gonadal context (Corre et al., 2016; Vousden et al., 2018).

To date, we lack a formal comparison of SCD effects on the human and murine brain, which would be valuable for several reasons. First, it would provide a well-defined setting to develop new tools for formally comparing neuroanatomical changes between species, which we lack to date. Addressing this gap could accelerate comparative neuroscience more generally. Second, formally assessing homology of SCD effects between species is crucial for specifying the ways in which mouse models of SCD could serve to model mechanistic aspects of SCA in humans. Third, the unusual synteny of X-chromosome between humans and mice (Carver and Stubbs, 1997) increases the translational potential for exploring cross-species homology in gene dosage alterations. Indeed, there are several obstacles to mechanistic dissection of these effects in humans, including, but not limited to, the inaccessibility of the human brain, the difficulty in uncoupling SCD from gonadal effects, and environmental variation. The sex chromosome trisomy (SCT) mouse model produces XXY, XYY, XY, and XX mice with either a gonadal male (testes) or female (ovaries) background (Chen et al., 2013). Importantly, the model has been shown to recapitulate metabolic and motor features found in humans with sex chromosome trisomies (SCTs; Chen et al., 2013); however, the neuroanatomical effects have neither been characterized in this model nor compared with human SCT effects. Fourth, although SCTs are defined by an abnormal number of sex chromosomes, they provide a rare means of asking whether foundational sex-biased biological factors, namely, X- and Y-chromosome count, are associated with similar brain features in two different eutherian mammals.

Here, we use comparative neuroimaging in humans and murine cohorts with the same SCT variations, namely XXY and XYY, relative to XY controls, to assess the effect of an added X- or Y-chromosome on structural neuroimaging-derived global and regional brain volume. We evaluate the degree of spatial convergence between the effect of an added X- or Y-chromosome in each species. Finally, for a set of homologous human-mouse brain regions we assess the similarity of effects for an added X- or Y-chromosome across species. Our approach harnesses recent advances in neuroimaging methods leveraging high-field magnets that have allowed researchers to study the brain of rodents in a noninvasive way, acquiring comparable signal to that acquired in human neuroimaging studies (Denic et al., 2011; Dzietko et al., 2011; Hoyer et al., 2014). Our focus on structural magnetic resonance imaging (MRI)-derived phenotypes is motivated by (1) the known effects of sex and SCD on brain volume from both human and mouse neuroimaging studies (Corre et al., 2016; Raznahan et al., 2016; Qiu et al., 2018; Vousden et al., 2018) and (2) the advantages of using brain volume over behavioural measures for cross-species comparisons given the complexities of mapping human behavior in

nonhuman animals (Nestler and Hyman, 2010). Of note, although this current study applies a workflow for comparative neuroimaging to probe SCD effects, the methodological approaches we introduce can be generalized to aid comparative analysis of many other influences on brain anatomy.

## Materials and Methods

### Participants

The human sample in this study includes youth (aged 6–25 years) with one of two SCAs (XXY\_H or XYY\_H), each with their own completely independent euploid control (XY\_H) sample (XXY\_H,  $n = 99$ , XY\_H control,  $n = 82$ , and XYY\_H,  $n = 34$ , XY\_H controls,  $n = 37$ ). Independent control groups were acquired because of a scanner upgrade occurring between data collection of XXY and XYY cohorts. Additionally, the independence of control groups reduces the risk that effects observed in aneuploidy groups could be driven by the controls. Participants from the SCA groups were recruited through the National Institutes of Health (NIH) website and parental support groups, while healthy participants were recruited from the NIH Healthy Volunteer office. All participants underwent structural magnetic resonance imaging (MRI), and had normal radiologic reports, with no history of brain injury or neurologic disorders. Supernumerary X- and Y-chromosome carriage was confirmed by karyotype, and nonmosaicism was confirmed through visualization of 50 metaphase spreads in peripheral blood for XXY\_H and XYY\_H participants. XY\_H controls were screened to exclude a history of psychiatric or neurodevelopmental disorders. This study was approved by the NIH Combined Neuroscience Institutional Review Board. All participants gave consent or assent, as appropriate, and all protocols were completed at the NIH Clinical Center in Bethesda, Maryland (see Table 1 for demographics information).

### Mice

The sex chromosome trisomy (SCT) mouse model (Chen et al., 2013) is generated by mating XXY<sup>-</sup> gonadal females with XY<sup>-</sup>(Sry<sup>+</sup>) gonadal males. The testis-determining gene, *Sry*, is deleted from the Y-chromosome (Lovell-Badge and Robertson, 1990), preventing formation of testes and causing development of ovaries in XXY<sup>-</sup> mothers. The XY<sup>-</sup>(Sry<sup>+</sup>) father possesses an *Sry* transgene on chromosome 3, causing differentiation of testes. (Mahadevaiah et al., 1998; De Vries et al., 2002; Arnold and Chen, 2009). The XXY<sup>-</sup> mothers produce X and XY<sup>-</sup> eggs, while the XY<sup>-</sup>(Sry<sup>+</sup>) fathers produce X or Y sperm cells each with or without *Sry* (Chen et al., 2013). This yields eight potential genotypes: XX, XY, XXY, and XYY, each genotype with either testes or ovaries. In order to mirror the human SCT groups, gonadal male XY\_M ( $n = 18$ ), XXY\_M ( $n = 17$ ), and XYY\_M ( $n = 20$ ) mice were included in this study. All experiments were approved by the University of California, Los Angeles (UCLA) Animal Research Committee. Mice were group-housed at the UCLA animal facility based on gonadal sex, maintained at 23°C on a 12/12 h light/dark cycle, and fed regular chow diet with 5% fat *ad libitum* (LabDiet 5001).

### Human neuroimaging

#### Neuroimaging data acquisition

High-resolution MPRAGE T1-weighted (T1w) sMRI scans were acquired on each participant using a MR750 3-Tesla (General Electric) whole-body scanner with a 32-channel head coil (176 contiguous sagittal slices with  $256 \times 256$  in-plane matrix and 1-mm slice thickness yielding 1-mm isotropic voxels). T1w sMRI scans were converted from DICOM to Nifti and organized according to the Brain Imaging Data Structure (BIDS) using *heudiconv*.

#### Data processing

The BIDS compatible FreeSurfer pipeline (version 7.1.0; Fischl, 2012) was used for cortical and subcortical segmentation of the T1w MRI scans ([https://github.com/Shotgunosine/freesurfer/tree/fs\\_7](https://github.com/Shotgunosine/freesurfer/tree/fs_7)), which is documented and freely available for download online (<http://surfer.nmr.mgh.harvard.edu/>). The technical details of these procedures are described in prior publications (Dale and Sereno, 1993; Fischl et al., 1998, 1999, 2001,

**Table 1. Demographics for human sample**

Characteristic	XY	XXY	Statistics	XY	XYY	Statistics
Sample size	82	99		37	34	
Age (years)						
Mean	16.41	16.38	$F_{(1,179)} = 0.001, p = 0.973$	14.74	15.49	$F_{(1,69)} = 0.414, p = 0.522$
SD	5.77	4.78		4.53	5.33	
Range	6.03–24.99	6.67–25.8		5.6–24.7	7–25.9	
Full scale IQ						
Mean	114.9	93.25	$F_{(1,179)} = 137, p < 2e-16^{**}$	117.62	87.15	$F_{(1,69)} = 137.6, p < 2e-16^{**}$
SD	12.59	12.22		9.4	12.40a	
Range	83–146	64–127		97–136	62–111	
Socioeconomic status (SES)						
Mean	38.39	47.34	$F_{(1,179)} = 9.543, p = 0.0023^*$	38.89	54.91	$F_{(1,69)} = 17.16, p = 9.57e-05^{**}$
SD	17.87	20.6		14.47	18.04	
Range	20–95	20–120		20–70	20–95	

\* $p < 0.01$  and \*\* $p < 0.001$  for ANOVA test of significant difference between groups (XY vs XXY or XY vs XYY).

2002, 2004a,b; Dale et al., 1999; Fischl and Dale, 2000; Kuperberg et al., 2003; Desikan et al., 2006; Han et al., 2006; Jovicich et al., 2006; Reuter et al., 2010). Cortical surface reconstruction was achieved using the automated *recon-all* processing stream. From the surfaces, several features were extracted using the *mri\_anatomic\_stats* utility (cortical thickness, surface area, cortical volume, mean curvature, Gaussian curvature, intrinsic curvature index, and folding index). We focused on cortical volume to use a homologous measure across the human and mouse analyses. Vertex-level cortical volume measures were averaged across 360 cortical parcels from the Glasser Human Connectome Project regional parcellation, a highly detailed, multimodally informed cortical atlas (Glasser et al., 2016). The Euler number was extracted from each individual's cortical reconstruction. This is thought to reflect image quality and topological complexity. Participants with a Euler number less than  $-217$  were excluded from statistical analyses as this has been previously shown to be a robust quality control threshold and a proxy for in-scanner motion (Rosen et al., 2018). In automatic subcortical segmentation, also part of the automated *recon-all* processing stream, each voxel in the normalized brain volume is assigned one of  $\sim 40$  labels using FreeSurfer "aseg" feature (version 7.1.0; for full details, see Fischl et al., 2002, 2004a). The boundaries of regions are estimated based on expected shapes of structural and signal intensity from the T1w image. Each scan was visually inspected to exclude images that were corrupted by motion artifacts or had segmentation errors.

## Mouse neuroimaging

### Data acquisition

Young adult mice (postnatal day 65) were anesthetized, transcardially perfused, and decapitated at UCLA as previously described (Cahill et al., 2012), and shipped to the University of Toronto for scanning. Brains (kept within the skulls) were placed in a solution of paraformaldehyde (PFA) and Prohance (gadoteridol, Bracco Diagnostics Inc.) for fixation. A multichannel 7.0-T scanner with a 40-cm diameter bore magnet (Varian Inc.) was used to acquire MR images at 40- $\mu$ m-isotropic resolution (Spencer Noakes et al., 2017) for 16 brain samples concurrently (Dzai et al., 2011). Scan parameters: T2W 3D FSE cylindrical *k*-space acquisition sequence, TR/TE/ETL = 350 ms/12 ms/6, two averages, FOV/matrix-size = 20  $\times$  20  $\times$  25 mm/504  $\times$  504  $\times$  630, total-imaging-time = 14 h (Spencer Noakes et al., 2017).

### Data processing

Structural MRI images ( $n = 55$ ) were aligned by unbiased deformation-based morphometry using a previously described (Spring et al., 2007; Lerch et al., 2011) registration pipeline (Collins et al., 1994; Avants et al., 2009; Friedel et al., 2014). Briefly, all individual scans are registered together using affine and nonlinear registration to create a study-specific average/template, from which log-transformed Jacobian determinants can be calculated (Chung et al., 2001), quantifying the voxel-wise volumetric differences between each individual image and the study specific average/template. The MAGeT brain algorithm (Chakravarty et al., 2013; Pipitone et al., 2014) was used to segment images according to a published atlas of

355 unique regions (Dorr et al., 2008; Richards et al., 2011; Ullmann et al., 2013; Steadman et al., 2014).

## Statistical analysis

### Effects of sex chromosome aneuploidy on regional brain volume

**Human.** All statistical analyses were performed in R version 3.6.0. Volumes for each aneuploidy group were z-scored using the mean and SD measures of their independent XY\_H control group. For each case-control pair, we evaluated the effects of SCT on the volume of each cortical and subcortical brain structure using a linear model to assess the effect of group ( $\beta_1$ : XXY\_H vs XY\_H or XYY\_H vs XY\_H), with mean-centered age ( $\beta_2$ ), and total tissue volume (TTV;  $\beta_3$ ) as covariates ( $\epsilon$ : error term). The  $\beta$ -value for the group effect ( $\beta_1$ ) is referred to hereafter as a standardized effect size as it was computed on standardized (z-scored volumes). Test statistics were corrected for multiple comparisons using the false discovery rate (FDR) correction (Benjamini and Hochberg, 1995; Benjamini and Yekutieli, 2001) with  $q$  (the expected proportion of false positives) set at 0.05. The formula, using region of interest (ROI)\_volume as the example region:

$$\text{XXY\_H model: ROI\_volume} \sim \text{intercept} + \beta_1(\text{Group XXY\_H vs XY\_H}) + \beta_2(\text{age} - \text{mean age}) + \beta_3(\text{TTV})$$

$$\text{XYY\_H model: ROI\_volume} \sim \text{intercept} + \beta_1(\text{Group XYY\_H vs XY\_H}) + \beta_2(\text{age} - \text{mean age}) + \beta_3(\text{TTV})$$

**Mouse.** To mirror the human analyses, volumes for all groups were z-scored using the mean and SD of the XY\_M control group. Effects of SCD on brain volume were again assessed using a linear model testing for the effect of group ( $\beta_1$ : XXY\_M or XYY\_M vs XY\_M control), with total tissue volume ( $\beta_2$ ) as a covariate ( $\epsilon$ : error term). Again, the  $\beta$ -value for group ( $\beta_1$ ) is referred to as a standardized effect size. Since there was a single control group, we ran a single linear model, comparing each SCT group to the XY control (set as the reference group). We did not covary for age in this model as the mice were of the same age.

$$\text{XXY\_M model: ROI\_volume} \sim \text{intercept} + \beta_1(\text{Group XXY\_M vs XY\_M}) + \beta_2(\text{TTV}) + \epsilon$$

$$\text{XYY\_M model: ROI\_volume} \sim \text{intercept} + \beta_1(\text{Group XYY\_M vs XY\_M}) + \beta_2(\text{TTV}) + \epsilon$$

We performed an additional analysis to test for the reproducibility of effects in XY, XXY, and XYY mice with ovaries [XY ( $n = 24$ ), XXY ( $n = 19$ ), and XYY ( $n = 22$ )]. We computed the standardized effect size

( $\beta_1$ ) for the effect of an added X- or Y-chromosome and correlated them with the standardized effect sizes computed for mice with testes across all brain regions. Additionally, in both species, analyses were repeated without TTV correction.

#### Spatial correlation and convergence of effects between XXY and XYY groups

**Human.** To assess the spatial convergence of the effects of adding an X- or adding a Y-chromosome on brain volume, the standardized effect size ( $\beta_1$  value) from the XXY\_H and XYY\_H models was correlated across all brain regions. Regions that were either consistently increased or decreased because of the addition of an X- or Y-chromosome were identified based on the sign of the standardized effect size coefficients in statistically significant regions.

**Mouse.** Since each mouse aneuploidy group did not have its own independent control group, we developed a resampling-based approach to formally test for spatial convergence of more subtle SCT effects in mice while ensuring independence of XY controls between murine SCT groups (to mirror the independence of XY controls for SCT groups in humans). Specifically, for each round of this analysis, we generated two independent XY control groups by repeatedly splitting the XY\_M control group ( $n = 18$ ) in half, Sample A ( $n = 9$ ) and Sample B ( $n = 9$ ), sampling without replacement. Regional effect sizes were estimated for XXY and XYY as compared with their respective XY control groups (sample A for XXY and sample B for XYY). For each control-split, and across all brain regions, we used a linear model to assess for group effects, with correction for total tissue volume. For each control split, the  $\beta_1$  was stored.

**Mouse model Samle A:** ROI\_volume  $\sim$  intercept

+  $\beta_1$ (Group XXY\_M vs XY\_SampleA)

+  $\beta_2$ (Total Brain Volume) +  $\epsilon$

**Mouse model Samle B:** ROI\_volume  $\sim$  intercept

+  $\beta_1$ (Group XYY\_M vs XY\_SampleB)

+  $\beta_2$ (Total Brain Volume) +  $\epsilon$

The standardized effect size ( $\beta_1$  value) of each brain region for sample A was correlated to that of Sample B across every region in the brain. This procedure was repeated 1000 times to (1) yield a distribution of estimates for the cross-region of interest (ROI) similarity in effect sizes of XXY and XYY on murine brain volume, and (2) identify any ROIs that showed a congruent direction of volume change in XXY and XYY across at least  $\geq 95\%$  of these iterations (950/1000 splits). We took any such regions to be instances of subthreshold convergence in the effects of XXY and XYY on regional murine brain volume. In both species, analyses were repeated without TTV correction. In mice, TTV-covaried analyses were also repeated in the ovarian murine group to screen for potentially reproducible sex chromosome dosage effects on regional brain volume in mice across both gonadal contexts.

#### Cross-species comparison for the effects of an added X- or Y-chromosome

Lastly, we sought to apply a direct test for the spatial convergence between SCT effects in humans and mice, separately for XXY and XYY. To this end, we restricted analysis to a subset of brain regions with well-established homology between humans and mice based on comparative studies, both structural and functional (Vogt and Paxinos, 2014; Glasser et al., 2016; Gogolla, 2017; Swanson and Hof, 2019; Balsters et al., 2020; Beauchamp et al., 2022), and a model proposed by Swanson and colleagues (Swanson and Hof, 2019), as well as the work of others (Vogt and Paxinos, 2014; Gogolla, 2017), which maps neuroanatomical regions based on six cytoarchitectonic and MRI-derived human atlases and three cytoarchitectonic mouse atlases (as well as two rat atlases). Human brain atlases include Brodmann (Brodmann, 1909, 1910) and Swanson (Swanson, 2015; cytoarchitectonic), and Desikan–Killiany (Desikan et al., 2006), Glasser (Glasser et al., 2016), and the Allen Institute for Brain Science (MRI-based). The Allen Brain Institute (Dong, 2008), Hof (Hof

et al., 2000), and Paxinos and Franklin (Paxinos and Franklin, 2019) were used as the mouse brain atlases. Based on this framework, we identified 21 brain regions determined to be homologous between humans and mice (Table 2). We repeated the procedure described in Statistical analysis to generate standardized effect sizes for group (covarying for total tissue volume for both species and mean-centered age for humans) using z-scored volumes relative to the XY\_H and XY\_M controls. The standardized effect sizes for the effect of adding an X-chromosome were correlated across species (XXY\_H with XYY\_M), as were those for adding a Y-chromosome (XYY\_H with XYY\_M). In both species, analyses were repeated without TTV correction.

## Results

### Comparing SCT effects on global brain volume in humans and mice

We first examined the effects of added X- or Y-chromosomes on total tissue volume (TTV) in humans (\_H) and mice (\_M). In humans volume was significantly decreased in XXY\_H ( $-4.3\%$ , 95% confidence interval (CI)  $[-5.6\%, -3.0\%]$ ;  $t = -6.429$ ,  $\beta = -0.944$ ,  $p = 1.14e^{-09}$ ), and nonsignificantly increased in XYY\_H ( $+1.5\%$ , 95% CI  $[-0.5\%, +3.4\%]$ ;  $t = 1.561$ ,  $\beta = 0.423$ ,  $p = 0.123$ ; Fig. 1A,C). In contrast, SCT had a negligible effect on TTV in mice, with slightly smaller volumes in both aneuploidy groups as compared with controls (XXY\_M vs XY\_M:  $-0.6\%$ , 95% CI  $[-2.1\%, +0.9\%]$ ;  $t = -0.789$ ,  $\beta = -0.285$ ,  $p = 0.436$ ; XYY\_M vs XY\_M:  $-0.7\%$ , 95% CI  $[-2.3\%, +0.9\%]$ ;  $t = -0.860$ ,  $\beta = -0.319$ ,  $p = 0.395$ ; Fig. 1B,D).

### Comparing SCT effects on regional brain volume in humans and mice

Next, we examined the effects of added X- or Y-chromosomes on regional gray matter volumes in each species. In humans, addition of a Y-chromosome induced a wider effect size range of regional brain volume changes than addition of an X-chromosome (Levene's test for variance difference in effect sizes:  $F_{(1,754)} = 34.214$ ,  $p = 7.349e^{-09}$ ; Fig. 2A), whereas the distribution of effect sizes for mice with added X- or Y-chromosomes was not different (Levene's test,  $F_{(1,906)} = 0.224$ ,  $p = 0.636$ ; Fig. 2B). For both XXY and XYY contrasts, the distribution of SCT effect sizes on regional brain volume was more variable in humans than mice (XXY:  $F_{(1,831)} = 14.091$ ,  $p = 0.0002$ ; XYY:  $F_{(1,831)} = 109.83$ ,  $p = 2.263 \times 10^{-16}$ ).

Humans showed several statistically-significant effects of SCT on regional cortical and subcortical volume after correction for multiple comparisons [using the false discovery rate (FDR) correction (Benjamini and Hochberg, 1995; Benjamini and Yekutieli, 2001) with  $q = 0.05$  and corresponding  $t$  value thresholds of XXY\_H:  $t = 2.678$ , XYY\_H:  $t = -2.528$ ]. We observed highly similar effects of XXY\_H and XYY\_H on regional brain anatomy. In humans, both SCTs induced statistically significant volume increases in the bilateral posterior parietal cortex (XXY\_H: 5m, 5mv, 5L, 7AL, and left 7PL, 7m, 7Am; XYY\_H: 5L, R5m, 7AL, R7Am, 7m), visual cortex (XXY\_H: V1, V2, and left V3, V7; XYY\_H: V1, V2, V3, L V3A, V4, V6, L V6A, V7, and prostriate cortex), dorsal visual transition area, parieto-occipital sulcus, intraparietal area, primary somatosensory cortex (XXY\_H: area 1, 2, 3b; XYY\_H: area 1, 2), and cingulate cortex (XXY\_H: 24dd; XYY\_H: v23ab, p24pr, 31pd). In both XXY\_H and XYY\_H, volume decreases were seen in the insular cortex (XXY\_H: MI, Ig, Pol1 and 2, AI, AAIC, R 52; XYY\_H: Pol1, MI, 52, R Pol2, L Ig, L AVI), temporal cortex (XXY\_H: TPOJ1 and 2, TA2, STGa, STSdp, and

**Table 2. Mapping of homologous human-mouse brain regions (TTV-corrected standardized effect sizes)**

Label	Human atlas (Glasser/FreeSurfer# names)	Mouse atlas	Hemisphere	Human (XXY_H)	Mouse (XXY_M)	Human (XYY_H)	Mouse (XYY_M)
Agranular insula	AVI, AAI, MI	Agranular insular area	L	−1.021*	0.216	−0.756*	−0.141
			R	−1.052*	0.299	−0.815*	0.125
Amygdala	Amygdala#	Cortical subplate	L	−0.423*	0.140	−0.350	−0.330
			R	−0.518*	−0.012	−0.595*	−0.073
Anterior cingulate area	A24pr, a24, p24pr, p24, 24dd, 24dv, p32pr, d32, a32pr, p32, s32	Anterior cingulate area	L	−0.141	−0.096	0.017	−0.087
			R	−0.134	−0.168	0.160	−0.067
Caudoputamen	Caudate#, Putamen#	Caudoputamen	L	−0.609*	0.241	−0.694*	0.144
			R	−0.762*	0.375	−0.671*	0.273
Cerebellar cortex	Cerebellar cortex#	Cerebellar cortex	L	−0.720*	−0.079	−0.923*	−0.302
			R	−0.792*	−0.223	−0.503*	−0.337
Entorhinal cortex	EC	Entorhinal area	L	0.129	0.005	0.576*	−0.349
			R	−0.082	−0.105	0.525	−0.371
Globus pallidus	Globus pallidus#	Pallidum	L	−0.670*	0.097	−0.837*	−0.001
			R	−0.704*	0.116	−0.860*	0.155
Hippocampus	Hippocampus#	Hippocampal region	L	−0.251*	0.113	−0.434*	−0.007
			R	−0.184	0.236	−0.151	0.138
Nucleus accumbens	Nucleus accumbens#	Striatum ventral region	L	−0.047	−0.028	−0.535*	−0.301
			R	−0.072	0.015	−0.231	−0.120
Perirhinal area	PeEc, TF, PHA2, PHA3	Perirhinal area	L	−0.143	0.635	0.250	−0.024
			R	−0.176	0.474	0.087	0.288
Piriform cortex	Pir	Piriform cortex	L	−0.705*	0.183	−0.415	−0.348
			R	−0.785*	−0.180	−0.586*	−0.266
Posterior parietal association areas	5m, 5mv, 5L	Posterior parietal association areas	L	0.853*	0.366	0.475*	0.189
			R	0.680*	−0.024	0.768*	−0.210
Primary auditory area	A1	Primary auditory area	L	0.062	0.141	0.177	0.176
			R	0.068	0.041	−0.265	0.377
Primary motor area	4	Primary motor area	L	0.219	−0.151	−0.014	−0.026
			R	−0.080	−0.173	0.299	−0.035
Primary somatosensory area	1, 2, 3a, 3b	Primary somatosensory area	L	0.591*	−0.063	0.179	0.117
			R	0.480*	−0.028	0.797*	−0.056
Primary visual area	V1	Primary visual area	L	0.555*	0.220	0.891*	−0.106
			R	0.439*	0.474	0.835*	−0.241
Retrosplenial area	RSC	Retrosplenial area	L	−0.187	−0.003	0.273	−0.148
			R	0.162	−0.219	0.709*	−0.326
Subiculum	PreS	Subiculum	L	−0.135	0.056	0.375	−0.128
			R	−0.241	0.166	−0.283	−0.051
Temporal association areas	FFC, PIT, TE1a, TE1p, TE2a, TF, STV, STSvp, STSva	Temporal association areas	L	−0.412*	0.246	−0.431*	−0.220
			R	−0.196	0.289	−0.444*	0.304
Thalamus	Thalamus#	Thalamus	L	−0.190	−0.031	−0.468	0.162
			R	−0.243	0.023	−0.471	0.259
Ventral orbital area	10r, 10v	Ventral orbital area	L	−0.043	−0.223	−0.099	0.028
			R	−0.012	−0.749	0.401	−0.416
Brain stem (midline)	Brainstem#	Midbrain, Hindbrain	M	−0.093	0.040	−0.742*	0.318
Total tissue volume (midline)	BrainSegVolNotVent#	Total tissue volume	M	0.000	0.000	0.000	0.000

Human = \_H; mouse = \_M.

Bold and \* denote regions that are statistically significantly different relative to controls.

bilateral PHT; XYY\_H: TE1p, PHT, R STSda, L TPOJ2), orbital part of inferior frontal gyrus (area 47), orbitofrontal cortex (OFC), fusiform face complex (bilateral in XXY\_H and only right hemisphere in XYY\_H), piriform cortex (bilateral in XXY\_H, and right hemisphere in XYY\_H), bilateral pallidum, and cerebellar cortex were observed in both human SCT groups. Despite this general picture of spatial convergence between significant XXY\_H and XYY\_H effects on regional brain volume, a few dissociations were seen. For example, XXY\_H individuals displayed greater increases in the posterior parietal cortex, particularly in the left hemisphere, while XYY\_H increases in the visual cortex were more prominent. Additional statistically significant volume decreases were observed in the bilateral putamen, pallidum, and amygdala for the XXY\_H group but not the XYY\_H group (Fig. 2D,E).

Mice lacked statistically significant effects of SCT on regional brain volumes after correction for multiple comparisons [using the false discovery rate (FDR) correction with  $q = 0.05$ ]. At a relaxed threshold (uncorrected  $p < 0.05$ ), we observed discordant effects of XXY and XYY, wherein XXY\_M had volume decreases in the accessory olfactory bulb and ventral retrosplenial area, specifically, the right cingulate cortex (area 29c), the right orbital area of XXY\_M, and in the right primary somatosensory area and the left paramedian lobule of the cerebellum, and volume increases in the perirhinal area, while XYY\_M had volume decreases in the primary somatosensory cortex and paramedian lobule of the cerebellum (Fig. 2F).

The SCT mouse model produces sex chromosome variations (e.g., XY, XXY, XYY) with either testes or ovaries (because of the presence or absence of the *Sry* transgene; Chen et al., 2013). Therefore, in mice only, we were able to further test the stability

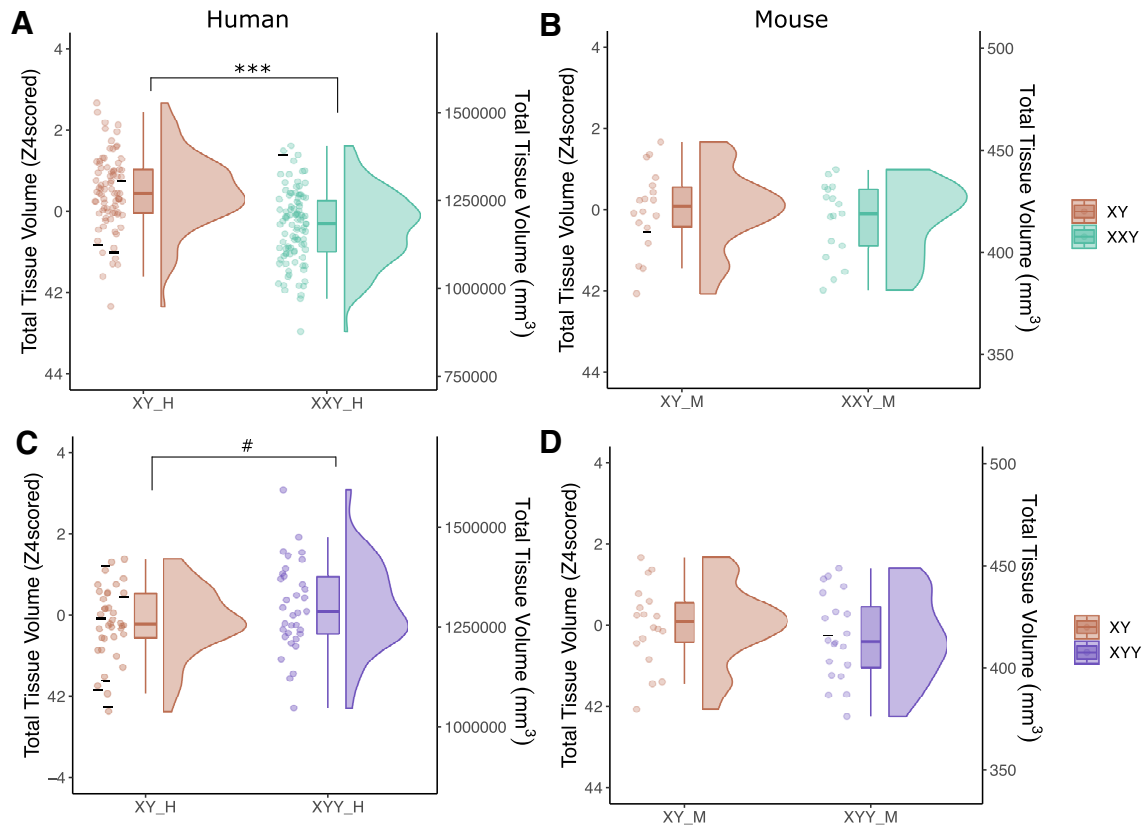


**Figure 1.** Effects of added X- or Y-chromosome on total tissue volume (TTV) in humans and mice. Distributions of TTV are shown for the effects of a supernumerary X- and Y-chromosome (**A, B** and **C, D**, respectively) in humans (**A, C**) and mice (**B, D**). Data are represented using individual points, boxplot, and half-violin plot (raincloud plot). \*\*\* $p < 0.0001$ , # $p = 0.123$ ; range of standardized effect sizes are as follows: XXY\_H group  $\beta = -1.10$  to  $+0.91$ ; XYY\_H  $\beta = -1.40$  to  $+1.31$ ; XXY\_M group  $\beta = -0.78$ - $0.61$ ; XYY\_M group  $\beta = -0.59$ - $0.47$ . Human = \_H; mouse = \_M.

of SCT effects on regional brain volume on an ovarian background (in addition to the testicular background necessarily used for our primary comparison of SCT effects in humans and mice). This additional test in mice revealed a moderately strong cross-regional correlation in the volumetric effects of XYY between ovarian and testicular groups ( $r = 0.56$ ) and a weaker cross-regional correlation in XXY effects ( $r = 0.22$ ); scatter plots for these effects are available online via FigShare (Guma, 2022a). Combining testicular and ovarian groups to model the main effects of XXY and XYY with increased power (controlling for gonadal type and TTV) revealed statistically significant decreases at 10% FDR in the olfactory bulbs of both XXY and XYY mice relative to XY (glomerular layer of the accessory olfactory bulb for XXY and right plexiform layer of the main olfactory bulb for XYY).

Repeating the above analyses without TTV correction did not reveal any statistically significant effects of SCT on regional brain volume in mice, and modified findings in humans such that significant brain-wide volume differences were observed in the XXY\_H group (driven by smaller TTV), while effects in XYY\_H were similar to those described above; a figure showing these results is available online via FigShare (Guma, 2022b). See Extended Data Tables 2-1 and 2-3 for human model outputs and Extended Data Tables 2-2 and 2-4 for mouse model outputs (with and without TTV correction).

#### Testing for convergent SCT effects in each species

The above results suggested that after correction for TTV effects, humans show statistically significant and largely convergent effects of XXY and XYY on regional brain volume, whereas mice

do not show statistically significant effects of SCT on regional brain volume. Based on the bootstrap analysis, the correlation of standardized effect sizes for each of the bootstrap resampled splits was low (cross-ROI mean  $r = -0.05$ ); the full distribution of these correlations across all 1000 splits available online via FigShare (Guma, 2022c). The cross-ROI correlation in effect sizes for XXY and XYY in humans was high (Fig. 3A,  $r = 0.73$ ), while in mice there did not appear to be a global alignment between the spatial pattern of XXY and XYY effects on regional brain volume (cross-ROI effect size correlation for a representative murine split, Fig. 3B,  $r = 0.073$ ). However, despite this lack of globally convergent XXY and XYY effects in mice, we identified several regions which showed convergent volume changes between XXY\_M and XYY\_M groups above chance levels ( $p < 0.05$ ). These regions allow a comparison with the regions of convergent statistically significant effects of XXY and XYY on regional volume in humans, which include increased volume in the posterior occipito-parietal regions and ventral anterior cingulate cortex, along with convergent volume decreases in insular, lateral temporal, orbitofrontal, piriform, fusiform face, pallidal, and cerebellar regions (Fig. 3C). In mice (Fig. 3D), we observed consistently overlapping volume increases in XXY\_M and XYY\_M versus XY\_M controls in the medial parietal association cortex (also increased in human SCT; Fig. 3E,I), right dorsal pallidum (decreased in human SCT; Fig. 3F, J), right CA1 and subiculum, right perirhinal area, and the periaqueductal gray. Conversely, consistent volume decreases with SCT in mice were seen in the olfactory bulbs (glomerular, mitral, and plexiform layers) as well as in the right cingulate cortex (29c; increased

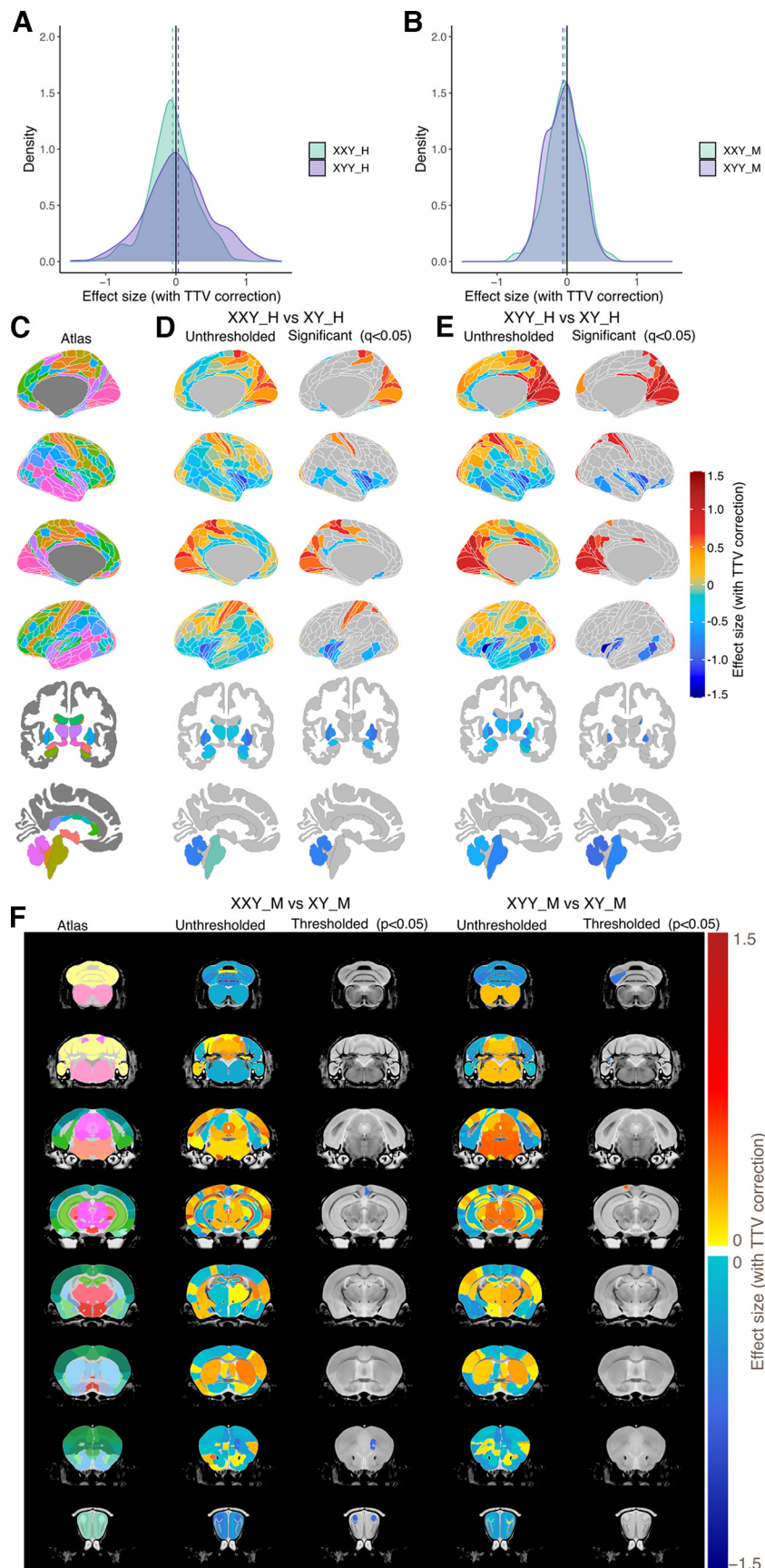


**Figure 2.** Effect of added X- or Y-chromosomes on regional brain volume in humans and mice, with total tissue volume (TTV) correction. Distribution of standardized effect sizes ( $\beta_1$ ) for the effect of sex chromosome trisomy are displayed for humans (A) and for mice (B). C, Representative views cortical Glasser atlas for lateral and medial slices of the left and right

in human SCT; Fig. 3G,K), right primary somatosensory cortex (increased in human SCT), right orbital area (also decreased in human SCT), and the left paramedian lobule of the cerebellum (also decreased in human SCT; Fig. 3H,L). We provide selected regional volume plots for SCT and XY groups from both humans (Fig. 3E–H) and mice (Fig. 3I,J) to illustrate the convergent and divergent neuroanatomical effects of SCT across species and highlight cross-species similarities and dissimilarities (Fig. 4).

Repeating the bootstrap conjunction analyses in mice (XXY, XYY, and XY) with ovaries provided an additional screen for consistent SCD effects on regional brain volume. This analysis revealed consistently overlapping volume increases in XXY\_F and XYY\_F versus XY\_F controls in the parietal association cortex, medial amygdalar nucleus, cingulate cortex (29c), primary visual area, and CA2, while consistently overlapping volume decreases were observed in the olfactory bulbs (glomerular and granular layers), primary and secondary motor cortex, right somatosensory cortex, and cingulate area (24b). Of note, several of these regions also showed overlapping effects of XXY and XYY in mice with testes, including increased parietal association cortex and decreased olfactory bulbs and somatosensory cortex, reinforcing the likelihood that these effects reflect direct and consistent convergent effects of supernumerary X- and Y-chromosome on regional brain volume in mice. Of these regions, the parietal association cortex also showed convergent volumetric effects of XXY and XYY in humans (Fig. 4).

Repeating the above tests for spatial convergence without covarying for TTV retained the strong spatial alignment between regional XXY and XYY effects in humans (cross-ROI effect size correlation  $r = 0.731$ ) and the lack of such an alignment in mice (cross-ROI correlation  $r = 0.024$ ). Regions showing a sub-threshold overlap in XXY and XYY-induced volume decreases in mice when not covarying for TTV included the cerebellum (paramedian lobule and crus 2), cortex (cingulate cortex area 29c, somatosensory cortex, orbital cortex, and prelimbic cortex), subcortex

←

hemispheres, and subcortical FreeSurfer atlas with both axial and sagittal views. Unthresholded (left) and significant ( $q < 0.05$ ; right) standardized effect sizes for the effect of added X-chromosome (D) and added Y-chromosome (E) in the human brain. F, Mouse brain coronal slices with the representative atlas on the left, followed by unthresholded, then thresholded ( $p < 0.05$ ) standardized effect sizes for the effect of added X-chromosome, followed by unthresholded, then thresholded ( $p < 0.05$ ) effects of added Y-chromosome. Human = \_H; mouse = \_M.

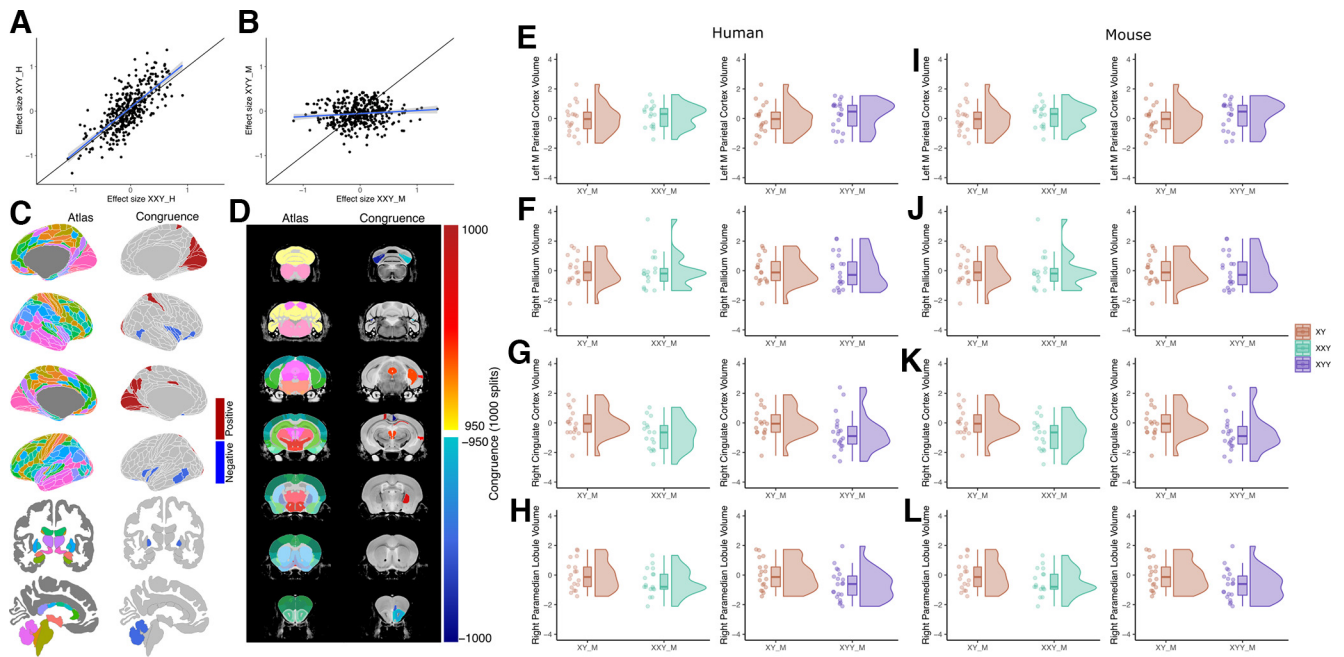


**Figure 3.** Spatial convergence between added X- or Y-chromosomes on the human and mouse brain. Standardized effect sizes for the effect of an added X- or added Y-chromosome are highly correlated across brain regions in humans (**A**), but not in mice [as illustrated by a representative split from the 1000 bootstraps (split 34; **B**)]. **C**, Human brain regions whose volume were either convergently increased (red;  $n = 22$ ) or consistently decreased (blue;  $n = 18$ ) in both aneuploidy groups. **D**, Mouse brain regions whose volume was consistently increased (red colors) or decreased (blue colors) in 95% (950/1000 splits) of the XY\_M control splits in both aneuploidy groups based on bootstrap analysis. Human anterior cingulate cortex (**E**) and parietal cortex (**F**) volume were convergently increased in both XXY\_H and XYY\_H, and cerebellum (**G**) and pallidum (**H**) volume were convergently decreased in both XXY\_H and XYY\_H. Mouse cingulate cortex (**I**), parietal cortex (**J**), cerebellum (**K**) volume was consistently and convergently decreased in both XXY\_M and XYY\_M, and pallidum (**L**) volume was consistently and convergently increased in both XXY\_M and XYY\_M. All plots use the standardized effect sizes for aneuploidy with total tissue volume correction. For all boxplots, volumes are standardized (z-scored relative to XY controls). Human = \_H; mouse = \_M.

(medial amygdalar nucleus), brainstem (right pontine reticular nucleus), and olfactory bulbs. A number of these regions align with those observed in the TTV-corrected analyses (cerebellum, somatosensory, cingulate, and orbital cortex, and olfactory bulb); however, a few additional regions emerge (prelimbic cortex, amygdalar nucleus, pontine reticular nucleus). Figure showing statistics for these comparisons are available online via FigShare (Guma, 2022d,e).

### Directly comparing the spatial pattern of SCT effects between species

We finally sought to achieve a direct test for the spatial convergence between SCT effects in humans and mice, separately for XXY and XYY. For both the effect of an added X- or Y-chromosome, there was low global similarity between the effects on the human and mouse brain based on low correlation of standardized effect sizes (added X-chromosome cross-ROI  $r = -0.07$ ; added Y-chromosome cross-ROI  $r = -0.26$ ; Fig. 5; Table 1). However, the direction of effect sizes in each species highlighted several regions of convergent SCT effects on brain volume in both species (albeit with larger effect sizes in humans than mice). Specifically, we found XXY-induced cross-species volume reductions in the right amygdala, bilateral anterior cingulate and cerebellar cortex, left nucleus accumbens, right piriform cortex, right primary motor area, left retrosplenial area, left thalamus, and bilateral ventral orbital, and cross-species volume increases in the left entorhinal cortex, left posterior parietal association area, bilateral primary auditory and primary visual areas. We found XYY-induced cross-species volume reductions in the bilateral amygdala, cerebellar cortex, left globus pallidus, left hippocampus, left nucleus accumbens, bilateral piriform

cortex, left primary motor area, right subiculum, and left temporal association area and cross-species volume increases in the right perirhinal area, left posterior association areas, left primary auditory and primary somatosensory areas (Table 2). The cross-species similarities in SCT effects were also low for standardized effect sizes that were not TTV-corrected; figure and table showing these results are available online via FigShare (Guma, 2022f,g).

### Discussion

This study provides the first cross-species comparison of the effects of an added X- or Y-chromosome on mammalian brain anatomy, leveraging a unique sample of human youth with SCT and young adult transgenic SCT mice. Our findings advance understanding of SCD effects on brain anatomy within and between species and take a first formalized step toward the broader topic of comparative neuroimaging of brain alterations between humans and mice. We consider each of these advances in turn below.

First, we detail the effects of two most common SCTs, Klinefelter syndrome (XXY) and Jacob's syndrome (XYY; Berglund et al., 2020) on global and regional brain volume in humans to model effects of SCD. The human results presented here provide the first analyses of regional brain volume in the SCA cohorts studied, and therefore offer the opportunity to assess replicability of findings compared with similar analyses in prior SCA cohorts (Shen et al., 2004; Steinman et al., 2009; Bryant et al., 2011; Hong et al., 2014; Raznahan et al., 2016; Reardon et al., 2016; Mankiw et al., 2017). Our findings align with those in prior SCA cohorts to provide an independent replication of several observations, including (1) a decrease in TTV with carriage of a supernumerary X-chromosome in males, (2) a trend toward greater TTV with carriage of

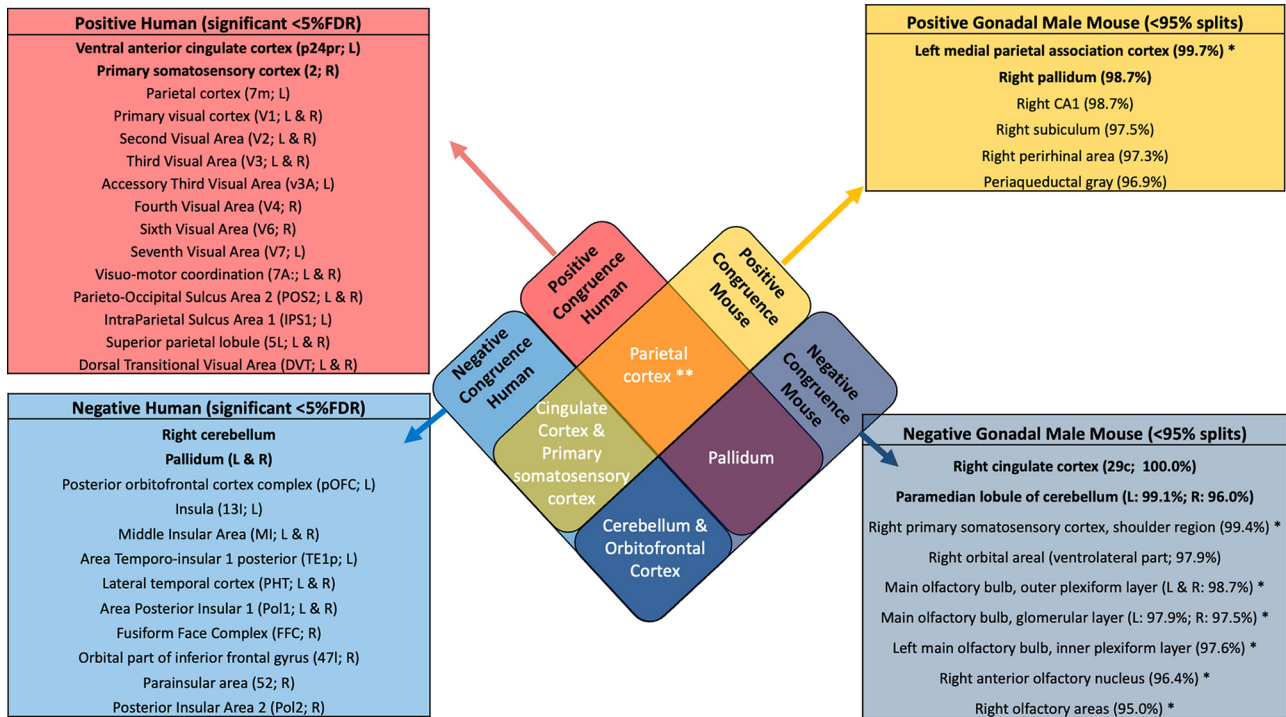


**Figure 4.** Convergetly increased or decreased regions in humans and mice. Venn diagram of overlapping regions of interest (ROIs) highlighting the regions congruently (for both XXY and XYY) increased or decreased in humans and mice. Brain regions that were statistically significantly impacted by both XXY and XYY in humans alone (<5%FDR) are listed in the red (increased volume) and light blue (decreased volume) boxes on the left. Brain regions that showed significantly convergent impacts of XXY and XYY (based on bootstrap resampling) in mice alone are listed in the yellow (increased volume) and dark blue (decreased volume) boxes. Intersection cells list regions showing convergent XXY and XYY effects in both species: orange, regions that are increased by XXY and XYY in both species; navy blue, regions that are decreased by XXY and XYY in both species; green, regions that are increased by XXY and XYY in mice, but decreased in humans; and purple, regions that are increases by XXY and XYY in humans, but decreased in mice. Human = *\_H*; mouse = *\_M*. Regions in bold are also highlighted in the central Venn diagram. \* Denotes regions that are affected in the same direction in Sex Chromosome Trisomy (SCT) mice with ovarian and testicular background, while \*\* denote regions that are affected in the same direction in humans as well as SCT mice with ovarian and testicular background.

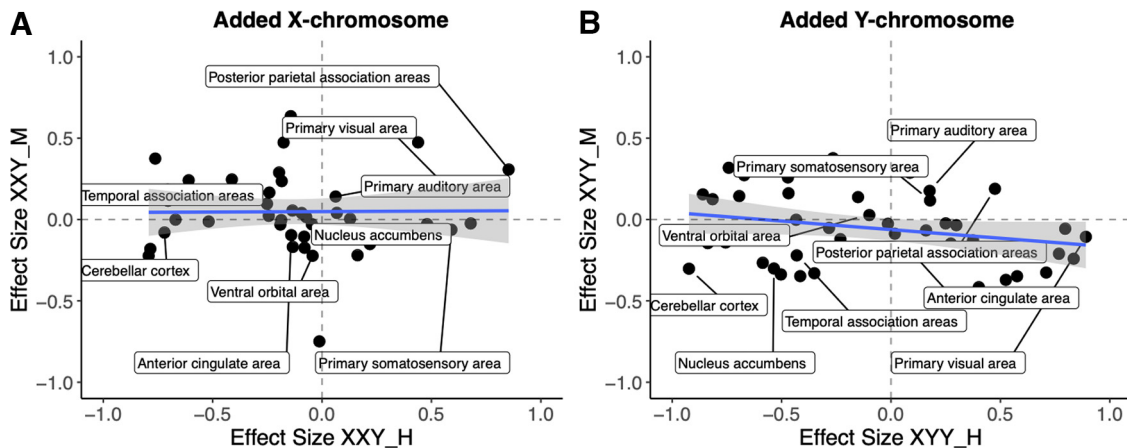


**Figure 5.** Correlation of effects of added X- or Y-chromosomes in human and mouse homologous brain regions. Standardized effect size correlation for the effect of (A) added X-chromosome (cross-ROI  $r = -0.07$ ) or (B) added Y-chromosome (cross-ROI  $r = -0.26$ ). Points are labeled only if they have the same directionality of standardized effect size in humans and mice (i.e., both positive or both negative). For simplicity, labels are for left hemisphere regions only as there were no large differences in laterality of effects. Human = *\_H*; mouse = *\_M*.

a supernumerary Y-chromosome, and (3) convergent effects of XXY and XYY on regional brain anatomy once these divergent global effects are controlled for. Convergent effects involve relative volumetric expansion of occipital and parietal cortices alongside relative volumetric contraction of insula and temporal cortices, cerebellum, brainstem, and basal ganglia. There is subtle variation within this general pattern of concordance between SCTs with slightly more pronounced volume contraction of the putamen, amygdala, piriform,

posterior cingulate, and frontal cortex in XXY and of the brainstem and auditory cortex in XYY. Differences in neuroanatomy could reflect differences in biology that distinguish these two SCTs. XXY individuals have higher total chromatin content and gene count than XYY (Snell and Turner, 2018). There may be differences in the expressed number of Y- and X-linked genes (especially those that escape X-inactivation; Skaletsky et al., 2003; Bellott et al., 2014; Deng et al., 2014; Raznahan and Disteche, 2021).

Secondary endocrine effects of XXY such as hypogonadism, low testosterone, and infertility (Ross et al., 2009), are not seen in XYY. The shared neuroanatomical effects of XXY and XYY could reflect biological features that these two aneuploidies have in common. Both SCTs lead to increased dosage of pseudoautosomal (PAR) and X-Y gametolog genes. It is also theoretically possible that generic effects of chromosomal trisomy explain shared neuroanatomical changes in XXY and XYY; however, this is countered by the fact that trisomy of chromosome 21 (Down syndrome) induces regional brain volume changes that differ from those seen in XXY or XYY (Seidlitz et al., 2020; Modenato et al., 2021).

Second, we provide the first systematic analysis of X- and Y-chromosome dosage effects on regional brain anatomy in mice. Carriage of an extra sex chromosome is associated with subtle neuroanatomical alterations in mice. Interestingly, the subtle effects of XXY and XYY on regional brain volume in mice showed weak and moderate stability, respectively, between independent groups differing in gonadal background, suggesting that some of these effects are capturing direct impact of SCD on neuroanatomy. Combining both gonadal groups revealed that XXY and XYY were both associated with reduced olfactory bulb volume after correction for multiple comparisons across regions. There are limited past studies of SCT effects on murine brain anatomy with which to compare our results. A previous neuroimaging study of XXY mice employing a different model (Raznahan et al., 2015) also identified enlarged periaqueductal gray volume and reduced olfactory bulb, retrosplenial, and somatosensory cortex strengthening the case for subtle but reproducible sensitivity of these regions to X-chromosome dosage.

Third, we formally compare SCT effects on brain anatomy between humans and mice and find a general lack of conservation of effects between species. Although sex chromosomes show privileged conservation between humans and mice (Carver and Stubbs, 1997; Graves et al., 2002) in terms of size and specific gene expression (Silkaitis and Lemos, 2014), there are differences between species. The male specific region of the Y-chromosome (MSY) has a larger proportion of ampliconic genes in mice compared with primates (Soh et al., 2014) resulting in degeneration of other genes (Soh et al., 2014). While most of the expanded mouse MSY gene families are expressed in the testes (Soh et al., 2014), they may indirectly explain some interspecies differences in Y-chromosome dosage on the brain. The X-chromosome has greater interspecies similarity than the Y; however, differences exist in gene location and presence of certain newly acquired genes (Sandstedt and Tucker, 2004; Deng et al., 2014). Mice also differ from humans in X-Y gene homology as (1) mice have only one small PAR, while humans have two larger PARs (Silkaitis and Lemos, 2014) and (2) mice have fewer Y-gametolog genes than humans (Martínez-Pacheco et al., 2020). Finally, the process of X-chromosome inactivation (XCI) and the degree of escape from XCI differs between species (Deng et al., 2014; Silkaitis and Lemos, 2014). Importantly, 12–15% of human and 3–5% of mouse genes escape consistently, and an additional 8–10% of human and 4% of mouse genes show variable tissue specific escape (Deng et al., 2014; Balaton et al., 2015; Snell and Turner, 2018). Given the putative importance of escape genes on brain volume (Nguyen and Disteche, 2006), these may influence species differences in X-chromosome dosage effects on the brain. There are also species differences in the autosomal context within which sex chromosomes operate, as well as in the evolutionary, developmental, and environmental contexts within which these genetic effects unfold.

Despite the general lack of similarity between SCT effects on the murine and human brain, our study design identified several regions that show convergent directional effects between SCTs and species. These include decreased cerebellum, orbital cortex volume and increased parietal association cortex volume. Of note, these parietal cortex effects were also apparent on an ovarian background in mice, underlining the strong candidacy of this region as a focus of conserved SCT effects on mammalian brain volume. These regions represent high priorities for follow-up studies aimed at understanding mechanistic effects of SCT on the brain, improving the translation between species.

Finally, our attempt to formalize a test of convergent anatomic effects of SCT on the human and murine brain raises several important insights for future comparative neuroimaging. We employed a parcellation-based approach; however, there are different ways of defining the units of analysis between species that go beyond classical anatomic nomenclature (subject to change based on parcellation; Eickhoff et al., 2018). Defining homology based on dominant functional systems—in the current context, visual systems in humans and the olfactory system in mice—goes beyond region-to-region comparison and considers an animal's environmental and evolutionary niche (Krubitzer and Prescott, 2018). This is an intriguing avenue of future research since SCT affects the human visual and the mouse olfactory system. Alignment across species may also be achieved by comparing patterns of homologous gene expression (Beauchamp et al., 2022), which reflect distinct patterns of molecular and morphometric neuroanatomical organization (Lein et al., 2007; Hawrylycz et al., 2012; Makowski et al., 2022) that is conserved between species (Strand et al., 2007; Hodge et al., 2019). Previous work has identified both homologous and divergent connections between human and macaque cortical circuits (Mars et al., 2016; van den Heuvel et al., 2019; Yokoyama et al., 2021) and human, macaque, and mouse cortico-striatal circuits (Balsters et al., 2020) by comparing connectivity patterns between brain regions. While structural MRI brings new opportunities to formalize cross-species testing as compared with other modalities such as behavior, there are inevitable species differences in lifestyle and sources of variance between laboratory mice (both inbred and outbred; Tuttle et al., 2018) and outbred humans.

Our results should be considered alongside some limitations. There may be ascertainment bias in the human SCT sample as patients presenting with more severe phenotypes are more likely to seek clinical attention and enroll in research (Bardsley et al., 2013; van Rijn 2019). Furthermore, the influence of environmental exposures and endocrine factors may confound effects in humans. Individuals with XXY typically have low testosterone levels, which can be corrected via hormone therapy (Tartaglia et al., 2010), both of which may impact brain anatomy (Savic et al., 2017). The human cohort was slightly younger than the mouse; mice were imaged in young adulthood (postnatal day 65), which is roughly equivalent to 20 years in humans (Dutta and Sengupta 2016), while the human sample ranged from ages 6–25 (mean age of 15 years). While many canonical sex differences arise during a critical period of sexual differentiation in neonatal development, sex differences do evolve through life in response to activational pubertal hormones among other developmental processes (McCarthy et al., 2012; Qiu et al., 2018). We control for age effects on human brain anatomy (we do not in the mouse as they are all the same age); however, it is possible that the slight age gap could result in some unaccounted differences between species. Another difference between species was that the human

imaging was performed *in vivo*, while the mouse imaging was performed *ex vivo* on fixed brains. Compared with *in vivo* imaging, *ex vivo* imaging allows for acquisition of higher resolution images with increased contrast- and signal-to-noise ratios compared with *in vivo* (Lerch et al., 2012). These advantages are accompanied by brain shrinkage, which has not been fully characterized with respect to uniformity across the brain (Cahill et al., 2012; Oguz et al., 2013; de Guzman et al., 2016; Holmes et al., 2017). However, notwithstanding this point, we would expect fixation procedures to affect all brains equally and not interfere with our ability to interpret between group differences (Cahill et al., 2012). Although our mouse sample was smaller than our human one, prior work suggests that our study design would be sufficiently powered to detect differences of a 0.25 effect size across the majority of brain regions (Holmes et al., 2017) including regional group differences of ~3% (Lerch et al., 2012; van Eede et al., 2013). Nevertheless, to further mitigate differences in sample size, we employ a resampling analysis and present differences using effect sizes as well as nominal p value thresholds. We base our species comparison solely on structure volume. Although the brain of both species is similarly organized, obtaining homology at a finer grain level is challenging, particularly for multimodal association cortices which show greater divergence between species (Laubach et al., 2018; Balsters et al., 2020). As discussed above, novel methods with which to formalize translation via transcriptional similarity (Beauchamp et al., 2022), or connectivity (Balsters et al., 2020; Mars et al., 2021) have shown great promise, and should be applied to the study of SCD in future work. Furthermore, integration of these findings across other mammals could enhance our understanding of the evolutionary pressures driving species differences in SCD effects on the brain; however, generating animal models (other than the mouse) with additional sex chromosomes may be a challenging endeavor.

In conclusion, our study shows that in humans, additional X-chromosomes and additional Y-chromosomes have divergent effects on TTV but large, and spatially similar effects on regional brain volume. In contrast, we observe subtle, and spatially dissimilar effects because of added X- or Y-chromosomes in the murine brain. Our screen of regional brain anatomy identified several regions which show similar directionality of volume change because of SCT in both humans and mice (e.g., cerebellar, parietal, and orbital cortex). These regions represent high-priority targets for future translational dissection of SCD effects on mammalian brain development, which may allow for a deeper mechanistic understanding of how SCD affects neuroanatomy. Establishing methods for cross-species comparison provides a promising avenue for better understanding the strengths and limitations of animal models in the study of the human brain in health and disease.

## References

- Arnold AP, Chen X (2009) What does the 'four core genotypes' mouse model tell us about sex differences in the brain and other tissues? *Front Neuroendocrinol* 30:1–9.
- Avants BB, Tustison N, Song G (2009) Advanced normalization tools (ANTS). *Insight J* 2:1–35.
- Balaton BP, Cotton AM, Brown CJ (2015) Derivation of consensus inactivation status for X-linked genes from genome-wide studies. *Biol Sex Differ* 6:35.
- Balsters JH, Zerbi V, Sallet J, Wenderoth N, Mars RB (2020) Primate homologies of mouse cortico-striatal circuits. *Elife* 9:e53680.
- Bardsley MZ, Kowal K, Levy C, Gosek A, Ayari N, Tartaglia N, Lahlou N, Winder B, Grimes S, Ross JL (2013) 47,XXX syndrome: clinical phenotype and timing of ascertainment. *J Pediatr* 163:1085–1094.
- Beauchamp A, Yee Y, Darwin B, Raznahan A, Mars RB, Lerch JP (2022) Whole-brain comparison of rodent and human brains using spatial transcriptomics. *elife* 11:e79418.
- Bellott DW, et al. (2014) Mammalian Y chromosomes retain widely expressed dosage-sensitive regulators. *Nature* 508:494–499.
- Benjamini Y, Hochberg Y (1995) Controlling the false discovery rate: a practical and powerful approach to multiple testing. *J R Stat Soc Series B Stat Methodol* 57:289–300.
- Benjamini Y, Yekutieli D (2001) The control of the false discovery rate in multiple testing under dependency. *Ann Statist* 29:1165–1188.
- Berglund A, Stochholm K, Gravholt CH (2020) The epidemiology of sex chromosome abnormalities. *Am J Med Genet C Semin Med Genet* 184:202–215.
- Brodman K (1909) Vergleichende Lokalisationslehre der Grosshirnrinde in Ihren Prinzipien Dargestellt auf Grund des Zellenbaues. Leipzig: Barth.
- Brodman K (1910) Feinere Anatomie Des Großhirns. In: *Handbuch der Neurologie. Monographien aus dem Gesamtgebiete der Neurologie und Psychiatrie*. Berlin; Heidelberg: Springer.
- Bryant DM, Hoefl F, Lai S, Lackey J, Roeltgen D, Ross J, Reiss AL (2011) Neuroanatomical phenotype of Klinefelter syndrome in childhood: a voxel-based morphometry study. *J Neurosci* 31:6654–6660.
- Cahill LS, Laliberté CL, Ellegood J, Spring S, Gleave JA, van Eede MC, Lerch JP, Henkelman RM (2012) Preparation of fixed mouse brains for MRI. *Neuroimage* 60:933–939.
- Carver EA, Stubbs L (1997) Zooming in on the human–mouse comparative map: genome conservation re-examined on a high-resolution scale. *Genome Res* 7:1123–1137.
- Chakravarty M, Mallar P, Steadman MC, van Eede MC, Calcott RD, Gu V, Shaw P, Raznahan A, Collins DL, Lerch JP (2013) Performing label-fusion-based segmentation using multiple automatically generated templates. *Hum Brain Mapp* 34:2635–2654.
- Chen X, Williams-Burris SM, McClusky R, Ngun TC, Ghahramani N, Barseghyan H, Reue K, Vilain E, Arnold AP (2013) The sex chromosome trisomy mouse model of XXY and XYY: metabolism and motor performance. *Biol Sex Differ* 4:15.
- Chung MK, Worsley KJ, Paus T, Cherif C, Collins DL, Giedd JN, Rapoport JL, Evans AC (2001) A unified statistical approach to deformation-based morphometry. *Neuroimage* 14:595–606.
- Collins DL, Neelin P, Peters TM, Evans AC (1994) Automatic 3D intersubject registration of MR volumetric data in standardized Talairach space. *J Comput Assist Tomogr* 18:192–205.
- Corre C, Friedel M, Vousden DA, Metcalf A, Spring S, Qiu LR, Lerch JP, Palmert MR (2016) Separate effects of sex hormones and sex chromosomes on brain structure and function revealed by high-resolution magnetic resonance imaging and spatial navigation assessment of the four core genotype mouse model. *Brain Struct Funct* 221:997–1016.
- Dale AM, Sereno MI (1993) Improved localization of cortical activity by combining EEG and MEG with MRI cortical surface reconstruction: a linear approach. *J Cogn Neurosci* 5:162–176.
- Dale AM, Fischl B, Sereno MI (1999) Cortical surface-based analysis. *Neuroimage* 9:179–194.
- Dzaji J, Spring S, Cahill LS, Mark Henkelman R (2011) Multiple-mouse neuroanatomical magnetic resonance imaging. *J Vis Exp* (48):2497.
- Deng X, Berletch JB, Nguyen DK, Distche CM (2014) X chromosome regulation: diverse patterns in development, tissues and disease. *Nat Rev Genet* 15:367–378.
- Denic A, Macura SI, Mishra P, Gamez JD, Rodriguez M, Pirko I (2011) MRI in rodent models of brain disorders. *Neurotherapeutics* 8:3–18.
- Desikan RS, Ségonne F, Fischl B, Quinn BT, Dickerson BC, Blacker D, Buckner RL, Dale AM, Maguire RP, Hyman BT, Albert MS, Killiany RJ (2006) An automated labeling system for subdividing the human cerebral cortex on MRI scans into gyral based regions of interest. *Neuroimage* 31:968–980.
- De Vries GJ, Rissman EF, Simerly RB, Yang L-Y, Scordalakes EM, Auger CJ, Swain A, Lovell-Badge R, Burgoyne PS, Arnold AP (2002) A model system for study of sex chromosome effects on sexually dimorphic neural and behavioral traits. *J Neurosci* 22:9005–9014.
- Dong HW (2008) The Allen reference atlas: a digital color brain atlas of the C57Bl/6J male mouse. New York: John Wiley and Sons.
- Dorr AE, Lerch JP, Spring S, Kabani N, Henkelman RM (2008) High resolution three-dimensional brain atlas using an average magnetic resonance image of 40 adult C57Bl/6J mice. *Neuroimage* 42:60–69.
- Dutta S, Sengupta P (2016) Men and mice: relating their ages. *Life Sci* 152:244–248.

- Dzietko M, Wendland M, Derugin N, Ferriero DM, Vexler ZS (2011) Magnetic resonance imaging (MRI) as a translational tool for the study of neonatal stroke. *J Child Neurol* 26:1145–1153.
- van Eede MC, Scholz J, Chakravarty MM, Henkelman RM, Lerch JP (2013) Mapping registration sensitivity in MR mouse brain images. *Neuroimage* 82:226–236.
- Eickhoff SB, Thomas Yeo BT, Genon S (2018) Imaging-based parcellations of the human brain. *Nat Rev Neurosci* 19:672–686.
- Fischl B (2012) FreeSurfer. *Neuroimage* 62:774–781.
- Fischl B, Dale AM (2000) Measuring the thickness of the human cerebral cortex from magnetic resonance images. *Proc Natl Acad Sci U S A* 97:11050–11055.
- Fischl B, Dale AM, Sereno MI, Tootell RBH, Rosen BR (1998) A coordinate system for the cortical surface. *Neuroimage* 7:5740.
- Fischl B, Sereno MI, Tootell RB, Dale AM (1999) High-resolution intersubject averaging and a coordinate system for the cortical surface. *Hum Brain Mapp* 8:272–284.
- Fischl B, Liu A, Dale AM (2001) Automated manifold surgery: constructing geometrically accurate and topologically correct models of the human cerebral cortex. *IEEE Trans Med Imaging* 20:70–80.
- Fischl B, Salat DH, Busa E, Albert M, Dieterich M, Haselgrove C, van der Kouwe A, Killiany R, Kennedy D, Klaveness S, Montillo A, Makris N, Rosen B, Dale AM (2002) Whole brain segmentation: automated labeling of neuroanatomical structures in the human brain. *Neuron* 33:341–355.
- Fischl B, van der Kouwe A, Destrieux C, Halgren E, Ségonne F, Salat DH, Busa E, Seidman LJ, Goldstein J, Kennedy D, Caviness V, Makris N, Rosen B, Dale AM (2004a) Automatically parcellating the human cerebral cortex. *Cereb Cortex* 14:11–22.
- Fischl B, Salat DH, van der Kouwe AJ, Makris N, Ségonne F, Quinn BT, Dale AM (2004b) Sequence-independent segmentation of magnetic resonance images. *Neuroimage* 23(Suppl 1):S69–S84.
- Friedel M, van Eede MC, Pipitone J, Chakravarty MM, Lerch JP (2014) Pydipper: a flexible toolkit for constructing novel registration pipelines. *Front Neuroinform* 8:67.
- Glasser MF, Coalson TS, Robinson EC, Hacker CD, Harwell J, Yacoub E, Ugurbil K, Andersson J, Beckmann CF, Jenkinson M, Smith SM, Van Essen DC (2016) A multi-modal parcellation of human cerebral cortex. *Nature* 536:171–178.
- Gogolla N (2017) The insular cortex. *Curr Biol* 27:R580–R586.
- Graves JAM, Géczy J, Hameister H (2002) Evolution of the human X—a smart and sexy chromosome that controls speciation and development. *Cytogenet Genome Res* 99:141–145.
- Guma E (2022a) Similarity of SCT effects on neuroanatomy across gonadal background. *figshare*. Figure. Available at [https://figshare.com/articles/figure/Similarity\\_of\\_SCT\\_effects\\_on\\_neuroanatomy\\_across\\_gonadal\\_background\\_/21728138/1](https://figshare.com/articles/figure/Similarity_of_SCT_effects_on_neuroanatomy_across_gonadal_background_/21728138/1).
- Guma E (2022b) Effect of added X- or Y-chromosomes on regional brain volume in humans and mice, without total tissue volume (TTV) correction. *figshare*. Figure. Available at [https://figshare.com/articles/figure/Effect\\_of\\_added\\_X-\\_or\\_Y-\\_chromosomes\\_on\\_regional\\_brain\\_volume\\_in\\_humans\\_and\\_mice\\_without\\_total\\_tissue\\_volume\\_TTV\\_correction/21728117/1](https://figshare.com/articles/figure/Effect_of_added_X-_or_Y-_chromosomes_on_regional_brain_volume_in_humans_and_mice_without_total_tissue_volume_TTV_correction/21728117/1).
- Guma E (2022c) Bootstrap analysis shows low spatial correlation for effects of an added X- or Y-chromosome in the mouse brain. *figshare*. Figure. Available at [https://figshare.com/articles/figure/Bootstrap\\_analysis\\_shows\\_low\\_spatial\\_correlation\\_for\\_effects\\_of\\_an\\_added\\_X-\\_or\\_Y-\\_chromosome\\_in\\_the\\_mouse\\_brain/21728159/1](https://figshare.com/articles/figure/Bootstrap_analysis_shows_low_spatial_correlation_for_effects_of_an_added_X-_or_Y-_chromosome_in_the_mouse_brain/21728159/1).
- Guma E (2022d) Spatial convergence between added X- or Y-chromosomes on the human and mouse brain without total tissue volume (TTV) correction. *figshare*. Figure. Available at [https://figshare.com/articles/figure/Spatial\\_convergence\\_between\\_added\\_X-\\_or\\_Y-\\_chromosomes\\_on\\_the\\_human\\_and\\_mouse\\_brain\\_without\\_total\\_tissue\\_volume\\_TTV\\_correction/21728144/1](https://figshare.com/articles/figure/Spatial_convergence_between_added_X-_or_Y-_chromosomes_on_the_human_and_mouse_brain_without_total_tissue_volume_TTV_correction/21728144/1).
- Guma E (2022e) Convergently increased or decreased regions in humans and mice without total tissue volume (TTV) correction. *figshare*. Figure. Available at [https://figshare.com/articles/figure/Convergently\\_increased\\_or\\_decreased\\_regions\\_in\\_humans\\_and\\_mice\\_without\\_total\\_tissue\\_volume\\_TTV\\_correction/21728171/1](https://figshare.com/articles/figure/Convergently_increased_or_decreased_regions_in_humans_and_mice_without_total_tissue_volume_TTV_correction/21728171/1).
- Guma E (2022f) Correlation of effects of added X- or Y-chromosomes in human and mouse homologous brain regions when total tissue volume (TTV) is not controlled for. *figshare*. Figure. Available at [https://figshare.com/articles/figure/Correlation\\_of\\_effects\\_of\\_added\\_X-\\_or\\_Y-\\_chromosomes\\_in\\_human\\_and\\_mouse\\_homologous\\_brain\\_regions\\_when\\_total\\_tissue\\_volume\\_TTV\\_is\\_not\\_controlled\\_for/21728186/1](https://figshare.com/articles/figure/Correlation_of_effects_of_added_X-_or_Y-_chromosomes_in_human_and_mouse_homologous_brain_regions_when_total_tissue_volume_TTV_is_not_controlled_for/21728186/1).
- Guma E (2022g) Mapping of homologous human-mouse brain regions (standardized effect sizes with TTV correction). *figshare*. Figure. Available at [https://figshare.com/articles/figure/Mapping\\_of\\_homologous\\_human-mouse\\_brain\\_regions\\_standardized\\_effect\\_sizes\\_with\\_TTV\\_correction\\_/21728477/1](https://figshare.com/articles/figure/Mapping_of_homologous_human-mouse_brain_regions_standardized_effect_sizes_with_TTV_correction_/21728477/1).
- de Guzman AE, Wong MD, Gleave JA, Nieman BJ (2016) Variations in post-perfusion immersion fixation and storage alter MRI measurements of mouse brain morphometry. *Neuroimage* 142:687–695.
- Han X, Jovicich J, Salat D, van der Kouwe A, Quinn B, Czanner S, Busa E, Pacheco J, Albert M, Killiany R, Maguire P, Rosas D, Makris N, Dale A, Dickerson B, Fischl B (2006) Reliability of MRI-derived measurements of human cerebral cortical thickness: the effects of field strength, scanner upgrade and manufacturer. *Neuroimage* 32:180–194.
- Hawrylycz MJ, et al. (2012) An anatomically comprehensive atlas of the adult human brain transcriptome. *Nature* 489:391–399.
- Hodge RD, et al. (2019) Conserved cell types with divergent features in human versus mouse cortex. *Nature* 573:61–68.
- Hof PRWG, Young FE, Bloom PV, Belichenko MR Celio (2000) Mouse brains. Comparative cytoarchitectonic atlas of the C57BL/6 and 129/SV. Amsterdam: Elsevier Science.
- Holmes HE, Powell NM, Ma D, Ismail O, Harrison IF, Wells JA, Colgan N, O’Callaghan JM, Johnson RA, Murray TK, Ahmed Z, Heggnes M, Fisher A, Cardoso MJ, Modat M, O’Neill MJ, Collins EC, Fisher EM, Ourselin S, Lythgoe MF (2017) Comparison of in vivo and ex vivo MRI for the detection of structural abnormalities in a mouse model of tauopathy. *Front Neuroinform* 11:20.
- Hong DS, Hoefft F, Marzelli MJ, Lepage J-F, Roeltgen D, Ross J, Reiss AL (2014) Influence of the X-chromosome on neuroanatomy: evidence from Turner and Klinefelter syndromes. *J Neurosci* 34:3509–3516.
- Hoyer C, Gass N, Weber-Fahr W, Sartorius A (2014) Advantages and challenges of small animal magnetic resonance imaging as a translational tool. *Neuropsychobiology* 69:187–201.
- Jovicich J, Czanner S, Greve D, Haley E, van der Kouwe A, Gollub R, Kennedy D, Schmitt F, Brown G, Macfall J, Fischl B, Dale A (2006) Reliability in multi-site structural MRI studies: effects of gradient non-linearity correction on phantom and human data. *Neuroimage* 30:436–443.
- Krubitzer LA, Prescott TJ (2018) The combinatorial creature: cortical phenotypes within and across lifetimes. *Trends Neurosci* 41:744–762.
- Kuperberg GR, Broome MR, McGuire PK, David AS, Eddy M, Ozawa F, Goff D, West WC, Williams SC, van der Kouwe AJ, Salat DH, Dale AM, Fischl B (2003) Regionally localized thinning of the cerebral cortex in schizophrenia. *Arch Gen Psychiatry* 60:878.
- Laubach M, Amarante LM, Swanson K, White SR (2018) What, if anything, is rodent prefrontal cortex? *eNeuro* 5:ENEURO.0315-18.2018.
- Lein ES, et al. (2007) Genome-wide atlas of gene expression in the adult mouse brain. *Nature* 445:168–176.
- Lerch JP, Yiu AP, Martinez-Canabal A, Pekar T, Bohbot VD, Frankland PW, Henkelman RM, Josselyn SA, Sled JG (2011) Maze training in mice induces MRI-detectable brain shape changes specific to the type of learning. *Neuroimage* 54:2086–2095.
- Lerch JP, Gazdzinski L, Germann J, Sled JG, Henkelman RM, Nieman BJ (2012) Wanted dead or alive? The tradeoff between in-vivo versus ex-vivo MR brain imaging in the mouse. *Front Neuroinform* 6:6.
- Lovell-Badge R, Robertson E (1990) XY female mice resulting from a heritable mutation in the primary testis-determining gene, Tdy. *Development* 109:635–646.
- Mahadevaiah SK, Odorisio T, Elliott DJ, Rattigan A, Szot M, Laval SH, Washburn LL, McCarrey JR, Cattanaach BM, Lovell-Badge R, Burgoyne PS (1998) Mouse homologues of the human AZF candidate gene RBM are expressed in spermatogonia and spermatids, and map to a Y chromosome deletion interval associated with a high incidence of sperm abnormalities. *Hum Mol Genet* 7:715–727.
- Makowski C, van der Meer D, Dong W, Wang H, Wu Y, Zou J, Liu C, Rosenthal SB, Hagler DJ Jr, Fan CC, Kremen WS, Andreassen OA, Jernigan TL, Dale AM, Zhang K, Visscher PM, Yang J, Chen CH (2022) Discovery of genomic loci of the human cerebral cortex using genetically informed brain atlases. *Science* 375:522–528.
- Mankiw C, Park MTM, Reardon PK, Fish AM, Clasen LS, Greenstein D, Giedd JN, Blumenthal JD, Lerch JP, Chakravarty MM, Raznahan A (2017) Allometric analysis detects brain size-independent effects of sex

- and sex chromosome complement on human cerebellar organization. *J Neurosci* 37:5221–5231.
- Mars RB, Verhagen L, Gladwin TE, Neubert F-X, Sallet J, Rushworth MFS (2016) Comparing brains by matching connectivity profiles. *Neurosci Biobehav Rev* 60:90–97.
- Mars RB, Jbabdi S, Rushworth MFS (2021) A common space approach to comparative neuroscience. *Annu Rev Neurosci* 44:69–86.
- Martínez-Pacheco M, Tenorio M, Almonte L, Fajardo V, Godínez A, Fernández D, Cornejo-Páramo P, Díaz-Barba K, Halbert J, Liechti A, Székely T, Urrutia AO, Cortez D (2020) Expression evolution of ancestral XY gametologs across all major groups of placental mammals. *Genome Biol Evol* 12:2015–2028.
- McCarthy MM, Arnold AP, Ball GF, Blaustein JD, De Vries GJ (2012) Sex differences in the brain: the not so inconvenient truth. *J Neurosci* 32:2241–2247.
- Modenato C, Martin-Brevet S, Moreau CA, Rodríguez-Herreros B, Kumar K, Draganski B, Sønderby IE, Jacquemont S (2021) Lessons learned from neuroimaging studies of copy number variants: a systematic review. *Biol Psychiatry* 90:596–610.
- Nestler EJ, Hyman SE (2010) Animal models of neuropsychiatric disorders. *Nat Neurosci* 13:1161–1169.
- Nguyen DK, Disteche CM (2006) High expression of the mammalian X chromosome in brain. *Brain Res* 1126:46–49.
- Oguz I, Yaxley R, Budin F, Hoogstoel M, Lee J, Maltbie E, Liu W, Crews FT (2013) Comparison of magnetic resonance imaging in live vs. post mortem rat brains. *PLoS One* 8:e71027.
- Paxinos G, Franklin KBJ (2019) Paxinos and Franklin's the mouse brain in stereotaxic coordinates. San Diego: Academic Press.
- Pipitone J, Park MTM, Winterburn J, Lett TA, Lerch JP, Pruessner JC, Lepage M, Voineskos AN, Chakravarty MM; Alzheimer's Disease Neuroimaging Initiative (2014) Multi-atlas segmentation of the whole hippocampus and subfields using multiple automatically generated templates. *Neuroimage* 101:494–512.
- Qiu LR, Fernandes DJ, Szulc-Lerch KU, Dazai J, Nieman BJ, Turnbull DH, Foster JA, Palmert MR, Lerch JP (2018) Mouse MRI shows brain areas relatively larger in males emerge before those larger in females. *Nat Commun* 9:2615.
- Raznahan A, Disteche CM (2021) X-chromosome regulation and sex differences in brain anatomy. *Neurosci Biobehav Rev* 120:28–47.
- Raznahan A, Lue Y, Probst F, Greenstein D, Giedd J, Wang C, Lerch J, Swerdloff R (2015) Triangulating the sexually dimorphic brain through high-resolution neuroimaging of murine sex chromosome aneuploidies. *Brain Struct Funct* 220:3581–3593.
- Raznahan A, Lee NR, Greenstein D, Wallace GL, Blumenthal JD, Clasen LS, Giedd JN (2016) Globally divergent but locally convergent X- and Y-chromosome influences on cortical development. *Cereb Cortex* 26:70–79.
- Reardon PK, Clasen L, Giedd JN, Blumenthal J, Lerch JP, Chakravarty MM, Raznahan A (2016) An allometric analysis of sex and sex chromosome dosage effects on subcortical anatomy in humans. *J Neurosci* 36:2438–2448.
- Reuter M, Rosas HD, Fischl B (2010) Highly accurate inverse consistent registration: a robust approach. *Neuroimage* 53:1181–1196.
- Richards K, Watson C, Buckley RF, Kurniawan ND, Yang Z, Keller MD, Beare R, Bartlett PF, Egan GF, Galloway GJ, Paxinos G, Petrou S, Reutens DC (2011) Segmentation of the mouse hippocampal formation in magnetic resonance images. *Neuroimage* 58:732–740.
- Rosen AFG, Roalf DR, Ruparel K, Blake J, Seelaus K, Villa LP, Ciric R, Cook PA, Davatzikos C, Elliott MA, Garcia de La Garza A, Gennatas ED, Quarmley M, Schmitt JE, Shinohara RT, Tisdall MD, Craddock RC, Gur RE, Gur RC, Satterthwaite TD (2018) Quantitative assessment of structural image quality. *Neuroimage* 169:407–418.
- Ross JL, Zeger MPD, Kushner H, Zinn AR, Roeltgen DP (2009) An extra X or Y chromosome: contrasting the cognitive and motor phenotypes in childhood in boys with 47,XYY syndrome or 47,XXY Klinefelter syndrome. *Dev Disabil Res Rev* 15:309–317.
- Sandstedt SA, Tucker PK (2004) Evolutionary strata on the mouse X chromosome correspond to strata on the human X chromosome. *Genome Res* 14:267–272.
- Savic I, Frisen L, Manzouri A, Nordenstrom A, Lindén Hirschberg A (2017) Role of testosterone and Y chromosome genes for the masculinization of the human brain. *Hum Brain Mapp* 38:1801–1814.
- Seidlitz J, Nadig A, Liu S, Bethlehem RAI, Vértes PE, Morgan SE, Váňa F (2020) Transcriptomic and cellular decoding of regional brain vulnerability to neurogenetic disorders. *Nat Commun* 11:3358.
- Shen D, Liu D, Liu H, Clasen L, Giedd J, Davatzikos C (2004) Automated morphometric study of brain variation in XXY males. *Neuroimage* 23:648–653.
- Silkaitis K, Lemos B (2014) Sex-biased chromatin and regulatory cross-talk between sex chromosomes, autosomes, and mitochondria. *Biol Sex Differ* 5:2.
- Skaletsky H, et al. (2003) The male-specific region of the human Y chromosome is a mosaic of discrete sequence classes. *Nature* 423:825–837.
- Snell DM, Turner JMA (2018) Sex chromosome effects on male–female differences in mammals. *Curr Biol* 28:R1313–R1324.
- Soh YQS, et al. (2014) Sequencing the mouse Y chromosome reveals convergent gene acquisition and amplification on both sex chromosomes. *Cell* 159:800–813.
- Spencer Noakes T, Henkelman RM, Nieman BJ (2017) Partitioning K-space for cylindrical three-dimensional rapid acquisition with relaxation enhancement imaging in the mouse brain. *NMR Biomed* 30:e3802.
- Spring S, Lerch JP, Henkelman RM (2007) Sexual dimorphism revealed in the structure of the mouse brain using three-dimensional magnetic resonance imaging. *Neuroimage* 35:1424–1433.
- Steadman PE, Ellegood J, Szulc KU, Turnbull DH, Joyner AL, Henkelman RM, Lerch JP (2014) Genetic effects on cerebellar structure across mouse models of autism using a magnetic resonance imaging atlas. *Autism Res* 7:124–137.
- Steinman K, Ross J, Lai S, Reiss A, Hoefl F (2009) Structural and functional neuroimaging in Klinefelter (47,XXY) syndrome: a review of the literature and preliminary results from a functional magnetic resonance imaging study of language. *Dev Disabil Res Rev* 15:295–308.
- Strand AD, Aragaki AK, Baquet ZC, Hodges A, Cunningham P, Holmans P, Jones KR, Jones L, Kooperberg C, Olson JM (2007) Conservation of regional gene expression in mouse and human brain. *PLoS Genet* 3:e59.
- Swanson LW (2015) Neuroanatomical terminology: a lexicon of classical origins and historical foundations. Oxford: Oxford University Press.
- Swanson LW, Hof PR (2019) A model for mapping between the human and rodent cerebral cortex. *J Comp Neurol* 527:2925–2927.
- Tartaglia NR, Ayari N, Howell S, Zeidler P (2010) Behavioral effects of testosterone therapy in adolescents with Klinefelter syndrome/XXY, XXYY, and XXXY: interim study results. *J Dev Behav Pediatr* 31:E1–E23.
- Tuttle AH, Philip VM, Chesler EJ, Mogil JS (2018) Comparing phenotypic variation between inbred and outbred mice. *Nat Methods* 15:994–996.
- Ullmann JF, Watson C, Janke AL, Kurniawan ND, Reutens DC (2013) A segmentation protocol and MRI atlas of the C57BL/6J mouse neocortex. *Neuroimage* 78:196–203.
- van den Heuvel MP, Scholtens LH, de Lange SC, Pijnenburg R, Cahn W, van Haren NEM, Sommer IE, Bozzali M, Koch K, Boks MP, Repple J, Pievani M, Li L, Preuss TM, Rilling JK (2019) Evolutionary modifications in human brain connectivity associated with schizophrenia. *Brain* 142:3991–4002.
- van Rijn S (2019) A review of neurocognitive functioning and risk for psychopathology in sex chromosome trisomy (47,XXY, 47,XXX, 47,YYY). *Curr Opin Psychiatry* 32:79–84.
- Vogt BA, Paxinos G (2014) Cytoarchitecture of mouse and rat cingulate cortex with human homologies. *Brain Struct Funct* 219:185–192.
- Vousden DA, Corre C, Spring S, Qiu LR, Metcalf A, Cox E, Lerch JP, Palmert MR (2018) Impact of X/Y genes and sex hormones on mouse neuroanatomy. *Neuroimage* 173:551–563.
- Yokoyama C, Autio JA, Ikeda T, Sallet J, Mars RB, Van Essen DC, Glasser MF, Sadato N, Hayashi T (2021) Comparative connectomics of the primate social brain. *Neuroimage* 245:118693.